Systematics of g factors of 2_1^+ states in even-even nuclei from Gd to Pt: A microscopic description by the projected shell model

Bao-An Bian[1,2], Yao-Min Di[1], Gui-Lu Long[3,1], Yang Sun[4,1], Jing-ye Zhang[5], Javid A. Sheikh[6]

[1]*Department of Physics, Xuzhou Normal University, Xuzhou, Jiangsu 221009, P.R. China*
[2]*Institute of Low Energy Nuclear Physics, Beijing Normal University, Beijing 100875, P. R. China*
[3]*Department of Physics, Tsinghua University, Beijing 100084, P.R. China*
[4]*Department of Physics and Joint Institute for Nuclear Astrophysics,*
University of Notre Dame, Notre Dame, Indiana 46556, USA
[5]*Department of Physics and Astronomy, University of Tennessee, Knoxville, Tennessee 37996, USA*
[6]*Department of Physics, University of Kashmir, Hazrathbal, Srinagar, Kashmir 190 006, India*
(Dated: February 9, 2008)

The systematics of g factor of first excited 2^+ state vs neutron number N is studied by the projected shell model. The study covers the even-even nuclei of all isotopic chains from Gd to Pt. g factors are calculated by using the many-body wavefunctions that reproduces well the energy levels and $B(E2)$s of the ground-state bands. For Gd to W isotopes the characteristic feature of the g factor data along an isotopic chain is described by the present model. Deficiency of the model in the g factor description for the heavier Os and Pt isotopes is discussed.

I. INTRODUCTION

Nuclear magnetic dipole moment can provide valuable information on the microscopic structure of a nuclear system. It is a sensitive probe of nuclear wavefunctions and hence can serve as a strict testing ground for theoretical models. Because of the intrinsically opposite signs of the neutron and proton g_s, a study of the gyromagnetic factor (g factor) enables determination of the detailed structure for underlying states. For example, variation of g factors often is a clear indicator for a single-particle component that strongly influences the total wavefunction. With advances in modern experimental techniques and sensitive detectors, progress in g factor measurement has continuously been made. In a recent paper [1], Berant *et al.*, by summarizing their new and the accumulated data from Refs. [2, 3], raised an interesting question on the systematic behavior of the first excited 2^+ g factors (denoted as $g(2_1^+)$ hereafter) in the rare earth nuclei and the heavier mass region. The data for these even-even nuclei indicate characteristic features of the systematics (see Fig. 4 below): with increasing neutron number, $g(2_1^+)$ factors display a decreasing trend in the Gd, Dy, and Er isotopes; stay nearly constant within a range of the Yb and Hf chains; then change to an increasing trend in the W and Os isotopes; but show a flat behavior in the Pt chain.

Clearly, the overall behavior of these g factors exhibits a large deviation from the rotor value, Z/A, which has only a very weak and smooth dependence on nucleon numbers [4]. On the other hand, the proton-neutron version of the Interacting Boson Model [5] gives an overly strong particle number dependence, and thus fails to reproduce the flat behavior of the g factors near the midshell [1]. These facts may suggest that in realistic nuclear systems, g factors reflect a delicate interplay between collective and single-particle degrees of freedom, which is dictated by the detailed shell structure. Very recently, Zhang *et al.* have discussed the systematical behavior of these $g(2_1^+)$ factors in terms of a simple phenomenological model [6]. However, it is desired that the $g(2_1^+)$ systematics can be described by microscopic theories. Spherical shell model calculation is applicable only to those heavy nuclei near the shell closures (for a recent example, see Ref. [7]). There have been microscopic models employed in the g factor calculation for heavy, deformed nuclei [8, 9, 10, 11, 12, 13, 14, 15]. However, except in Ref. [11], those calculations focused mainly on one or a few chosen examples in an isotopic chain. A microscopic description of the experimental $g(2_1^+)$ data for the large mass region as presented in Ref. [1] remains as a challenge to microscopic theories.

In the present article, we carry out a systematical study for $g(2_1^+)$ factors. As a theoretical tool, we employ the code developed in Ref. [12], which is based on the Projected Shell Model (PSM) [16]. In the PSM approach, one introduces axially deformed basis and performs exactly angular-momentum projection on the intrinsic states from deformed mean-field calculations. For even-even nuclei, angular-momentum projection on the lowest $K = 0$ state generates a rotational band, which is the main component of the ground-state band (g-band) including the 2_1^+ state of our interest. The lowest $K = 0$ state is the quasiparticle vacuum obtained microscopically through the Nilsson + BCS calculations in a large single-particle space. We thus expect this model to be an appropriate microscopic theory for the present investigation. The calculation is performed for nuclei from the Gd ($Z = 64$) to the Pt ($Z = 78$) isotopic chains, with neutron numbers ranging from $N = 88$ to 120. The nuclei studied here are known to have very different collective properties; for example, they can be well-deformed, less-deformed, or soft nuclei. The g factor of the first 2^+ state is dependent on details of the total wavefunction. The deviations from the collective Z/A trend are mainly

understood as a consequence of single-particle make-up of the wavefunction and the interplay between the collective degree of freedom and single particles. The present model employs deformed Nilsson single-particle states at fixed deformation. As we shall discuss, this scheme works well for well-deformed nuclei but is insufficient for description of soft nuclei in the heavier Os and Pt region.

II.   OUTLINE OF THE THEORY

A calculation for medium to heavy deformed nuclei in terms of the conventional (spherical) shell model is not feasible despite recent computational advances. The successful description of heavy deformed nuclei can be traced back to the introduction of the Nilsson potential [17]. In the Nilsson model, nuclear states are described by considering nucleons moving in a deformed potential. Deformed states are defined in the body-fixed frame of reference in which the rotational symmetry is broken. In order to calculate the observables, it is necessary to restore the broken rotational symmetry in the wavefunction. This can be done by using the standard angular momentum projection method. The projected states are then used to diagonalize a two-body shell model Hamiltonian. Thus, our approach follows closely with the basic philosophy of the conventional shell model. The main difference to the conventional shell model is that in the PSM, one starts with a deformed basis rather than a spherical one. For the details of the projection method, we refer to the PSM review article [16] and references cited therein.

The PSM constructs the shell-model space by using the axially symmetric Nilsson states with a quadrupole deformation ϵ_2. Pairing correlations are incorporated into the Nilsson states by the BCS calculations. The consequence of the Nilsson-BCS calculations defines a quasiparticle vacuum $|\Phi(\epsilon_2)\rangle \equiv |\Phi\rangle$ and the associated set of quasiparticle states in the intrinsic frame. For the low-lying nuclear states near the ground state the PSM wavefunction can be expressed as

$$\left|\Psi_M^I\right\rangle = f_{K=0}^I \, \hat{P}_{MK=0}^I \left|\Phi\right\rangle, \tag{1}$$

which is the angular-momentum-projected quasiparticle vacuum state with f being the normalization factor. In Eq. (1), $\hat{P}_{MK}^I$ is the angular-momentum-projection operator [18]

$$\hat{P}_{MK}^I = \frac{2I+1}{8\pi^2} \int d\Omega \, D_{MK}^I(\Omega) \, \hat{R}(\Omega). \tag{2}$$

As in the early PSM calculations, we use the pairing plus quadrupole-quadrupole (QQ) Hamiltonian with inclusion of the quadrupole-pairing term

$$\hat{H} = \hat{H}_0 - \frac{1}{2}\chi \sum_\mu \hat{Q}_\mu^\dagger \hat{Q}_\mu - G_M \hat{P}^\dagger \hat{P} - G_Q \sum_\mu \hat{P}_\mu^\dagger \hat{P}_\mu. \tag{3}$$

In Eq. (3), $\hat{H}_0$ is the spherical single-particle Hamiltonian, which contains a proper spin–orbit force [17]. As discussed in Ref. [16], the QQ-force strength χ is adjusted such that the quadrupole deformation ϵ_2 is obtained as a result of the self-consistent mean-field HFB calculation. The monopole pairing strength G_M is of the standard form $G_M = [20.12 \mp 13.13(N - Z)/A]/A$, with "$-$" for neutrons and "$+$" for protons, which approximately reproduces the observed odd–even mass differences in this mass region [16]. The quadrupole pairing strength G_Q is assumed to be proportional to G_M, with the proportionality constant being fixed to be 0.16 for all nuclei considered in this paper. The same constant has been used in the previous calculations for rare earth nuclei [16]. For the valence single-particle space, we have included three major shells, $N = 4, 5, 6$ (3,4,5), for neutrons (protons).

In short, the procedure of the present calculation is that based on a deformed Nilsson potential with pairing included in the BCS treatment, one performs explicit angular-momentum projection with a two-body interaction which conforms (through self-consistent conditions) with the mean-field Nilsson potential. The Hamiltonian with separable forces serves as an effective interaction, the strengths of which have been fitted to experimental data. The deformed single-particle states with deformation parameters ϵ_2 are used solely as a starting basis. It is sufficient for a calculation to have these deformation parameters close to the "true" nuclear deformation. Of course, a large departure from a true deformation would result in a significant enhancement in dimension of the configuration space, with the extreme case being the conventional shell model based on a spherical basis ($\epsilon_2 \equiv 0$).

III.   ENERGY LEVELS AND BE(2) VALUES

We study 61 nuclei from the Gd, Dy, Er, Yb, Hf, W, Os, and Pt isotopic chains. This large group includes nuclei with very different collective behavior. It is well-known that with neutron number around 90, nuclei are traditionally

TABLE I: The quadrupole deformation parameters with which the deformed bases are constructed.

| Z = 64	^{152}Gd	^{154}Gd	^{156}Gd	^{158}Gd	^{160}Gd					
ϵ_2	0.212	0.278	0.295	0.305	0.320					
Z = 66	^{154}Dy	^{156}Dy	^{158}Dy	^{160}Dy	^{162}Dy	^{164}Dy				
ϵ_2	0.200	0.240	0.260	0.270	0.280	0.290				
Z = 68	^{156}Er	^{158}Er	^{160}Er	^{162}Er	^{164}Er	^{166}Er	^{168}Er	^{170}Er		
ϵ_2	0.195	0.230	0.257	0.265	0.258	0.262	0.273	0.276		
Z = 70	^{164}Yb	^{166}Yb	^{168}Yb	^{170}Yb	^{172}Yb	^{174}Yb	^{176}Yb			
ϵ_2	0.245	0.250	0.260	0.265	0.269	0.266	0.263			
Z = 72	^{166}Hf	^{168}Hf	^{170}Hf	^{172}Hf	^{174}Hf	^{176}Hf	^{178}Hf	^{180}Hf		
ϵ_2	0.219	0.235	0.240	0.250	0.253	0.246	0.241	0.231		
Z = 74	^{168}W	^{170}W	^{172}W	^{174}W	^{176}W	^{178}W	^{180}W	^{182}W	^{184}W	^{186}W
ϵ_2	0.193	0.201	0.217	0.220	0.225	0.195	0.190	0.195	0.195	0.190
Z = 76	^{178}Os	^{180}Os	^{182}Os	^{184}Os	^{186}Os	^{188}Os	^{190}Os	^{192}Os		
ϵ_2	0.188	0.172	0.170	0.173	0.158	0.154	0.150	0.145		
Z = 78	^{182}Pt	^{184}Pt	^{186}Pt	^{188}Pt	^{190}Pt	^{192}Pt	^{194}Pt	^{196}Pt	^{198}Pt	
ϵ_2	0.197	0.187	0.175	0.135	0.128	0.116	0.113	0.120	0.170	
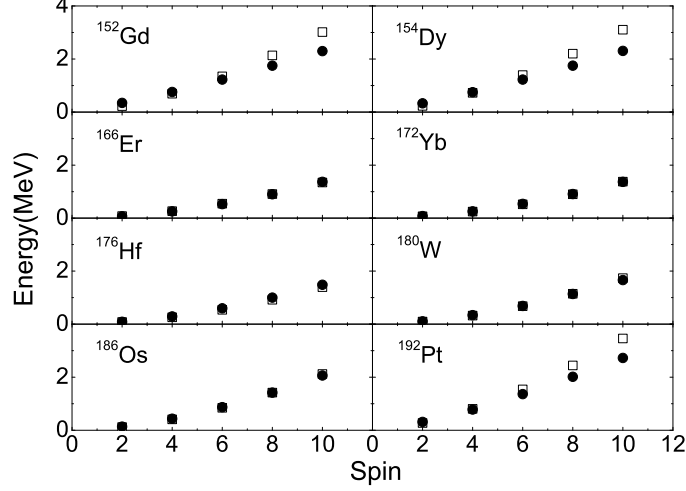
FIG. 1: Comparison of calculated energies with experimental data for g-bands. Open squares represent the calculated results and solid circles the data.

known as γ-soft nuclei. On the other hand, the heavier isotopes in the Os and Pt chains contain also significant γ-softness, and these are typical examples of $O(6)$ nuclei according to the Interacting Boson Model [19]. Between these two regions, nuclei are strongly deformed, for most of which the deformation is axial and the low-lying spectrum typically exhibits a rotor behavior. In Table I, we list the deformation parameters with which the deformed bases are constructed. The listed quadrupole deformations ϵ_2 agree with the systematic trend of those experimentally adopted ones [20] although the absolute values of ours are smaller. Note that it is not necessary for our input deformations to be exactly the same as those extracted from experiment as long as the so-constructed bases can correctly describe experimental $B(E2)$s (see Figs. 2 and 3 below). In the calculation, when the calculation condition is fixed we do not have a freedom to readjust the parameters to reproduce the g-factors. Namely, under a fixed calculation condition, g factors are predicted and the underlying physics is discussed.

Fig. 1 shows the calculated energy levels for g-bands together with experimental data. We include in the figure only one nucleus selected from each of the isotopic chains because all the calculations have achieved the same level of agreement. These examples are chosen to represent nuclei with distinct collective behavior. For instance, with neutron number 88, ^{152}Gd and ^{154}Dy are typical γ-soft nuclei lying in the transitional region. ^{166}Er, ^{172}Yb, and
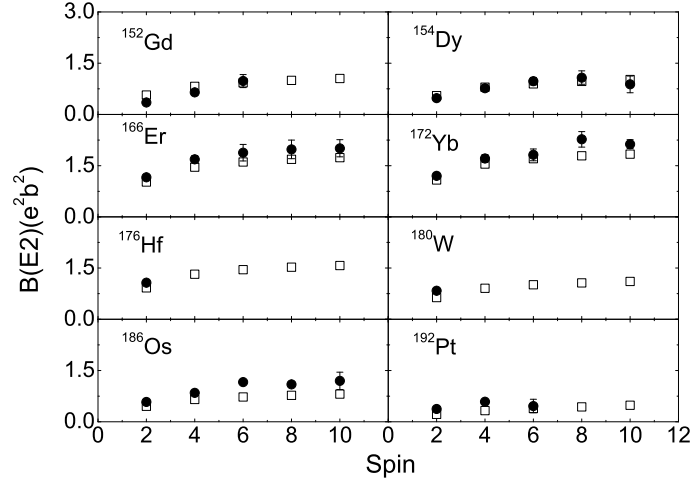
FIG. 2: Comparison of calculated g-band $B(E2)$ values with available data. Open squares represent the calculated results and solid circles (with error bars) the data.

^{176}Hf are representative examples of strongly deformed nuclei lying in the midshell, which have nearly constant moment of inertia. Finally, ^{186}Os and ^{192}Pt are again γ-soft in the transitional region. For all these nuclei with very different rotational behavior, it can be seen from Fig. 1 that the energy levels have been well reproduced by the calculation. Note that for the strongly deformed nuclei lying in the midshell, the energy intervals are considerably smaller, corresponding to larger moments of inertia in these nuclei. The deviation seen in the higher-spin states in ^{152}Gd, ^{154}Dy, and ^{192}Pt is caused by the g-band interactions with other configurations that have not been considered in Eq. (1).

We further calculate the g-band $B(E2)$ values for all nuclei studied in this paper using the same deformation parameters listed in Table I. The $B(E2)$ values that are related to an electric transition probability from an initial state I to a final state $I-2$ are given by

$$B(E2, I \rightarrow I-2) = \frac{1}{2I+1} |\langle \Psi^{I-2} ||\hat{Q}_2|| \Psi^I \rangle|^2 , \tag{4}$$

where wavefunctions $|\Psi^I\rangle$ are those in Eq. (1). The effective charges used in the calculation are the standard ones $e^\pi = 1.5e$ and $e^\nu = 0.5e$. The effective charges are fixed for all nuclei studied in this paper without any individual adjustment. Any variations in the calculated $B(E2)$ values, among one rotational band or between those in different nuclei, are subject to the structure change in wavefunctions. The calculation is compared with available data in Fig. 2. Again, we include in this figure only one nucleus selected from each of the isotopic chains, the same set of nuclei as shown in Fig. 1. It can be seen that the $B(E2)$ values are also nicely reproduced. Not only are the absolute values in each nucleus correctly given, but also the variations as a function of angular-momentum are described. We note in particular that the $B(E2)$s in ^{192}Pt are well reproduced; as we shall see later, for the Pt isotopic chain we encounter difficulties in the g-factor calculation.

In Fig. 3, we plot the calculated $B(E2, I = 2 \rightarrow I = 0)$ values for all the 61 nuclei considered in this work, and compare them with available data. The numbers used for the figure are listed in Table II. We stress that the variations in $B(E2)$ along each isotopic chain, i.e. a rapid increase up to $N \approx 94$, the flat behavior for $96 \leq N \leq 108$, and a decreasing trend after the midshell, are correctly described. A few local exceptions with rather large $B(E2)$ values in the data (such as in ^{172}W, ^{182}W, and ^{182}Os) can not be understood by the present calculation. The global trend of the $B(E2)$ values with exclusion of the Os and Pt chains has been discussed by a simple one-parameter model [6].

The agreement of the calculated $B(E2, I = 2 \rightarrow I = 0)$ values with data (Figs. 2 and 3) as well as the reproduction of the g-band energies (Fig. 1) indicate that under the present calculation conditions, we are able to describe the basic structure quantities for these nuclei. As far as the low-lying energy levels and $B(E2)$s are concerned, the method works well. The systematical agreement between the calculated and experimental $B(E2)$s (Fig. 3) justifies the use of the deformation parameters in Table I.
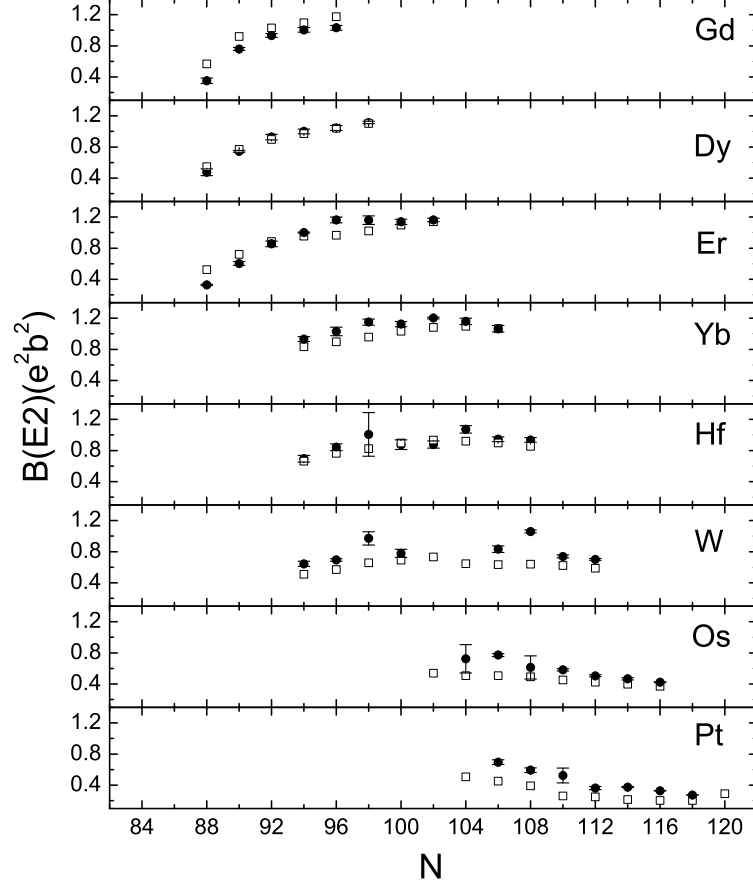
FIG. 3: Comparison of calculated $B(E2, I = 2 \to I = 0)$ with available data. Open squares represent the calculated results and solid circles (with error bars) the data.

IV. G-FACTOR RESULTS AND DISCUSSION

We now turn our discussion to g factors. In the PSM, g factors can be directly computed as

$$g(I) = \frac{\mu(I)}{\mu_N I} = \frac{1}{\mu_N I} \left[\mu_\pi(I) + \mu_\nu(I) \right], \tag{5}$$

with $\mu_\tau(I)$ being the magnetic moment of a state Ψ^I

$$
\begin{aligned}
\mu_\tau(I) &= \left\langle \Psi_I^I | \hat{\mu}_z^\tau | \Psi_I^I \right\rangle \\
&= \frac{I}{\sqrt{I(I+1)}} \left\langle \Psi^I || \hat{\mu}^\tau || \Psi^I \right\rangle \\
&= \frac{I}{\sqrt{I(I+1)}} \left[g_l^\tau \langle \Psi^I || \hat{j}^\tau || \Psi^I \rangle + (g_s^\tau - g_l^\tau) \langle \Psi^I || \hat{s}^\tau || \Psi^I \rangle \right],
\end{aligned}
\tag{6}
$$

where $\tau = \pi$ and ν for protons and neutrons, respectively.

We use the same wavefunctions that are used to evaluate $B(E2)$ values. In the angular-momentum-projection theory, the reduced matrix element for an operator $\hat{m}$ (with $\hat{m}$ being either $\hat{j}$ or $\hat{s}$ in Eq. (6)) can be explicitly

TABLE II: Comparison of calculated $B(E2, I = 2 \rightarrow I = 0)$ (in $e^2 b^2$) with available data.

Z = 64	^{152}Gd	^{154}Gd	^{156}Gd	^{158}Gd	^{160}Gd					
Exp.	0.35(3)	0.76(2)	0.93(3)	1.01(3)	1.03(3)					
Th.	0.57	0.92	1.03	1.09	1.18					

Z = 66	^{154}Dy	^{156}Dy	^{158}Dy	^{160}Dy	^{162}Dy	^{164}Dy				
Exp.	0.48(4)	0.75(1)	0.93(4)	1.00(3)	1.04(3)	1.11(2)				
Th.	0.55	0.77	0.90	0.97	1.04	1.10				

Z = 68	^{156}Er	^{158}Er	^{160}Er	^{162}Er	^{164}Er	^{166}Er	^{168}Er	^{170}Er		
Exp.	0.33(1)	0.60(3)	0.86(4)	1.00(5)	1.16(8)	1.16(5)	1.14(3)	1.16(2)		
Th.	0.52	0.72	0.89	0.96	0.97	1.02	1.10	1.14		

Z = 70	^{164}Yb	^{166}Yb	^{168}Yb	^{170}Yb	^{172}Yb	^{174}Yb	^{176}Yb			
Exp.	0.93(3)	1.03(5)	1.15(4)	1.12(3)	1.20(1)	1.16(4)	1.07(4)			
Th.	0.83	0.90	0.96	1.03	1.08	1.10	1.07			

Z = 72	^{166}Hf	^{168}Hf	^{170}Hf	^{172}Hf	^{174}Hf	^{176}Hf	^{178}Hf	^{180}Hf		
Exp.	0.69(4)	0.84(4)	1.01(30)	0.88(6)	0.88(5)	1.07(5)	0.95(3)	0.94(3)		
Th.	0.66	0.77	0.83	0.89	0.94	0.92	0.90	0.85		

Z = 74	^{168}W	^{170}W	^{172}W	^{174}W	^{176}W	^{178}W	^{180}W	^{182}W	^{184}W	^{186}W
Exp.	0.64(3)	0.69(2)	0.97(9)	0.78(5)			0.83(4)	1.06(2)	0.74(2)	0.70(1)
Th.	0.51	0.57	0.66	0.69	0.73	0.65	0.63	0.64	0.62	0.59

Z = 76	^{178}Os	^{180}Os	^{182}Os	^{184}Os	^{186}Os	^{188}Os	^{190}Os	^{192}Os		
Exp.		0.72(18)	0.77(2)	0.61(15)	0.58(2)	0.51(1)	0.47(1)	0.42(1)		
Th.	0.54	0.51	0.51	0.49	0.45	0.43	0.40	0.37		

Z = 78	^{182}Pt	^{184}Pt	^{186}Pt	^{188}Pt	^{190}Pt	^{192}Pt	^{194}Pt	^{196}Pt	^{198}Pt	
Exp.		0.70(3)	0.59(3)	0.53(9)	0.36(2)	0.38(1)	0.33(1)	0.27(1)		
Th.	0.51	0.45	0.39	0.26	0.25	0.22	0.20	0.20	0.29	

expressed as

$$
\begin{aligned}
\langle \Psi^I || \hat{m}^\tau || \Psi^I \rangle &= \sum_{K_i, K_f} f_{K_i}^I f_{K_f}^I \sum_{M_i, M_f, M} (-)^{I - M_f} \begin{pmatrix} I & 1 & I \\ -M_f & M & M_i \end{pmatrix} \langle \Phi | \hat{P}_{K_f M_f}^I \hat{m}_{1M} \hat{P}_{K_i M_i}^I | \Phi \rangle \\
&= (2I + 1) \sum_{K_i, K_f} (-)^{I - K_f} f_{K_i}^I f_{K_f}^I \sum_{M', M''} \begin{pmatrix} I & 1 & I \\ -K_f & M' & M'' \end{pmatrix} \\
&\quad \times \int d\Omega\, D_{M'' K_i}(\Omega) \langle \Phi | \hat{m}_{1M'} \hat{R}(\Omega) | \Phi \rangle.
\end{aligned}
$$

In our calculation, the following standard values for g_l and g_s appearing in Eq. (6) are taken:

$$
\begin{aligned}
g_l^\pi &= 1, & g_s^\pi &= 5.586 \times 0.75, \\
g_l^\nu &= 0, & g_s^\nu &= -3.826 \times 0.75.
\end{aligned}
$$

g_s^π and g_s^ν are damped by a usual 0.75 factor from the free-nucleon values to account for the core-polarization and meson-exchange current corrections [21]. The same values are used for all g factor calculations in the present paper, as in the previous projected shell model calculations, without any adjustment for individual nuclei.

We present the systematics of g factor of first 2^+ state for all the isotopic chains from Gd to Pt. In Fig. 4, a comparison of calculated results with available data [1, 2, 3] is given. The numbers used for the figure are listed in Table III. Interesting systematical features are clearly observed. The experimental $g(2_1^+)$ values of Gd, Dy, and Er isotopes show a downsloping trend with increasing neutron number N; those of heavier W and Os isotopes exhibit an upsloping behavior; and, according to the current set of data, the $g(2_1^+)$ factors of Yb, Hf and Pt isotopes are almost constant within each isotopic chain. From Fig. 4, it can be seen that the observed *trends* for the isotopic chains from Gd to W are qualitatively reproduced by the present calculation. Especially for most Dy, Er, and W nuclei, a quantitative agreement with data is achieved. The downsloping trend of Gd, Dy, and Er isotopes is well described. The calculation further predicts that for the Yb, Hf, and W isotopic chains, a downsloping trend is still visible for $N < 100$, but becomes nearly constant at the neutron midshell. The upsloping trend of W isotopes with $N \geq 106$ is well reproduced by the calculation. Nevertheless, there are cases where we find disagreement. We shall comment on those cases later.
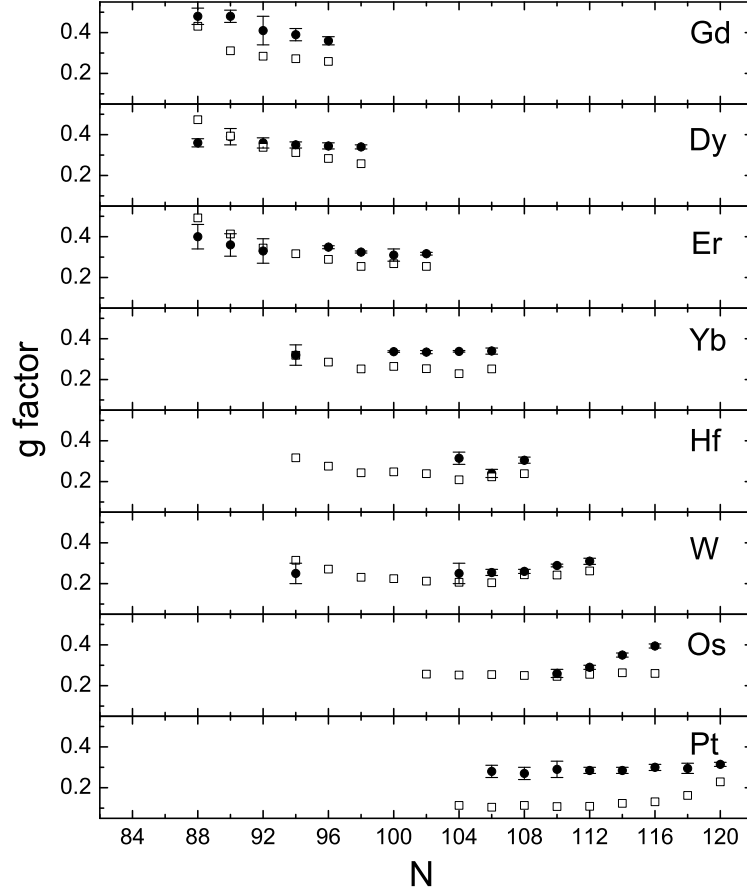
FIG. 4: Comparison of calculated 2^+ state g factor with available data. Open squares represent the calculated results and solid circles (with error bars) the data.

Fig. 5 shows the calculated $g(2_1^+)$ factors for Er and W isotopes. To understand the N-dependent variations, theoretical results are decomposed further into the individual contributions from the proton and neutron operator (see Eq. (5)), the sum of which is the total g factor that was compared with data in Fig. 4. Remarkably, we find that the $g(2_1^+)$ variations originate mostly from the proton contribution while the neutron contribution is very small and stays nearly constant within each of the isotopic chain. Therefore, the change of the proton contribution alone describes the observed variation trends of $g(2_1^+)$ factors, namely, a rapid decrease followed by a constancy in the Er nuclei and probably a U-shape in the W nuclei (see Fig. 5). It is rather interesting that the proton contribution varies as the neutron number changes along an isotopic chain. This can only be possible with the presence of strong neutron-proton interaction. In this regard, we notice that Zhang $et\ al.$ [6] suggested that the observed constancy of the $g(2_1^+)$ factors in the well-deformed region is attributed to the reduction of proton-neutron interaction strengths near the midshell.

While the calculation predicts a flat behavior of $g(2_1^+)$ for the lighter Os nuclei, a clear departure from data occurs for heavier Os isotopes and for all the Pt isotopes considered in this paper. Although for ^{198}Pt, the theoretical value becomes closer to the data, we must conclude that the present calculation fails to describe the observed $g(2_1^+)$ trend in the Os and Pt chains. We have tried various calculations by constructing our deformed model space with different ϵ_2 deformations. In the example of ^{192}Pt, it is found that with artificially increasing basis deformation, the $g(2_1^+)$ factor values starts going up, and at $\epsilon_2 = 0.24$ the calculated $g(2_1^+)$ agrees with data. However, the experimental energy levels and $B(E2)$ values in this nucleus cannot be simultaneously described. This may indicate that, although g-band energies and $B(E2)$s in the Os and Pt chains are reproduced by the model, the obtained wavefunctions with respect to the single-particle content can be wrong. We note that energy levels and $B(E2)$s near the ground state reflect mainly the collective properties of even-even nuclei and are not sensitive to single particles.

TABLE III: Comparison of calculated 2^+ state g factor with available data.

$Z = 64$	^{152}Gd	^{154}Gd	^{156}Gd	^{158}Gd	^{160}Gd
Exp.	0.48(4)	0.48(3)	0.41(7)	0.39(3)	0.36(2)
Th.	0.43	0.31	0.29	0.27	0.26

$Z = 66$	^{154}Dy	^{156}Dy	^{158}Dy	^{160}Dy	^{162}Dy	^{164}Dy
Exp.	0.36(2)	0.39(4)	0.36(3)	0.35(2)	0.35(2)	0.34(1)
Th.	0.47	0.39	0.34	0.31	0.28	0.26

$Z = 68$	^{156}Er	^{158}Er	^{160}Er	^{162}Er	^{164}Er	^{166}Er	^{168}Er	^{170}Er
Exp.	0.40(6)	0.36(6)	0.33(6)		0.349(8)	0.325(5)	0.31(3)	0.317(7)
Th.	0.49	0.41	0.35	0.32	0.29	0.25	0.27	0.26

$Z = 70$	^{164}Yb	^{166}Yb	^{168}Yb	^{170}Yb	^{172}Yb	^{174}Yb	^{176}Yb
Exp.	0.32(3)			0.337(4)	0.335(8)	0.338(4)	0.34(2)
Th.	0.32	0.29	0.25	0.26	0.25	0.23	0.25

$Z = 72$	^{166}Hf	^{168}Hf	^{170}Hf	^{172}Hf	^{174}Hf	^{176}Hf	^{178}Hf	^{180}Hf
Exp.						0.32(3)	0.24(2)	0.31(2)
Th.	0.32	0.28	0.24	0.25	0.24	0.21	0.22	0.24

$Z = 74$	^{168}W	^{170}W	^{172}W	^{174}W	^{176}W	^{178}W	^{180}W	^{182}W	^{184}W	^{186}W
Exp.	0.25(5)					0.25(5)	0.26(2)	0.26(1)	0.289(7)	0.31(2)
Th.	0.32	0.27	0.23	0.22	0.21	0.21	0.20	0.24	0.24	0.26

$Z = 76$	^{178}Os	^{180}Os	^{182}Os	^{184}Os	^{186}Os	^{188}Os	^{190}Os	^{192}Os
Exp.					0.26(2)	0.29(1)	0.35(1)	0.40(1)
Th.	0.26	0.26	0.25	0.25	0.25	0.26	0.26	0.26

$Z = 78$	^{182}Pt	^{184}Pt	^{186}Pt	^{188}Pt	^{190}Pt	^{192}Pt	^{194}Pt	^{196}Pt	^{198}Pt
Exp.		0.28(3)	0.27(3)	0.29(4)	0.29(2)	0.29(2)	0.30(2)	0.30(3)	0.32(1)
Th.	0.11	0.11	0.11	0.11	0.11	0.12	0.13	0.16	0.23

This calls for a further improvement of the projected shell model type approaches to generally describe transitional nuclei. More correlations in the wavefunction need to be included, which goes beyond what an axially deformed quasiparticle vacuum state can contain. These correlations can be introduced by the addition of the D-pair operators to the vacuum state [22], which takes both quasiparticle and collective degrees of freedom explicitly into account in a shell model basis. The generator coordinate method, which consists of a construction of a linear superposition of different product wave-functions, can also be adopted.

V. SUMMARY

Inspired by the recent experimental work of Berant *et al.,* [1], we have made an attempt to study systematically $g(2_1^+)$ for all the isotopes from Gd to Pt, using the projected shell model approach. With a single set of interaction strengths, we have carried out calculations for each nucleus in a projected basis constructed with appropriate deformations. We have been able to reproduce the energy levels and $B(E2)$s for low-lying states in the g-band for all the 61 nuclei considered in the paper. With the same set of calculation conditions, we have calculated g factors of the first 2^+ state. It has been found that for the isotopes from the Gd to W chain, the characteristics of experimental data along each isotopic chain are described by the theoretical calculations, such as the downsloping trend in the Gd, Dy, and Er isotopes, the upsloping trend in the W isotopes, and the flat behavior of the Yb and Hf isotopes. For the heavier Os and Pt nuclei, the results have indicated that although the energy levels and $B(E2)$s can be described equally well as in the lighter nuclei, the calculated g factors are wrong. Study of the separate contributions of proton and neutron to the $g(2_1^+)$ factors suggests that the variations of the g factors as the neutron number changes originate mainly from the proton contribution. The overly weak proton contribution to the g factors for Os and Pt isotopes indicates deficiency in the wavefunctions. To describe the heavier isotopes in the Os and Pt chains, improvement in the theory is required.
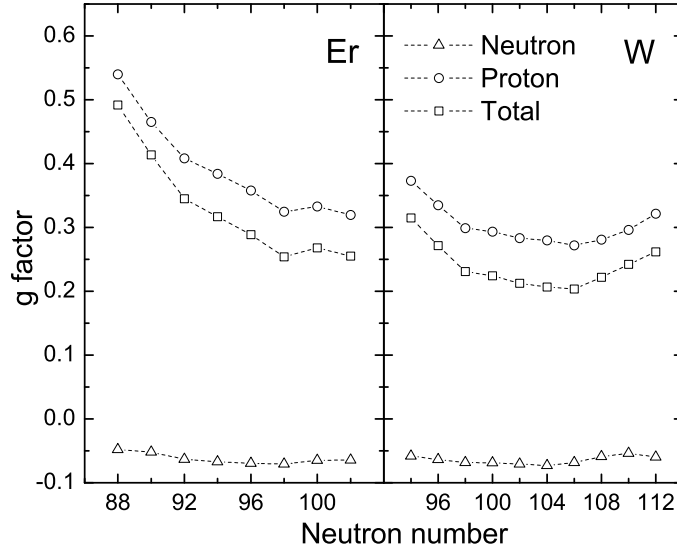
FIG. 5: Calculated first excited 2^+ state g factors for Er and W isotopes, with decomposition of the total g factor (open squares) into proton (open circles) and neutron (open triangles) contributions.

VI. ACKNOWLEDGMENTS

[1] Z. Berant, A. Wolf, N. V. Zamfir, M. A. Caprio, D. S. Brenner, N. Pietralla, R. L. Gill, R. F. Casten, C. W. Beausang, R. Krücken, C. J. Barton, J. R. Cooper, A. A. Hecht, D. M. Johnson, J. R. Novak, H. Cheng, B. F. Albanna, and G. Gurdal, Phys. Rev. C **69**, 034320 (2004).
[2] P. Raghavan, At. Data Nucl. Data Tables **42**, 189 (1989).
[3] N. J. Stone, Table of Nuclear Magnetic Dipole and Electric Quadrupole Moments, NNDC, http://www.BNL.gov (2001).
[4] W. Greiner, Nucl. Phys. **80**, 417 (1966).
[5] M. Sambataro, O. Scholten, A. E. L. Dieperink, and G. Piccito, Nucl. Phys. **A 423**, 333 (1984).
[6] J.-y. Zhang, R. F. Casten, A. Wolf, Z. Berant, R. B. Cakirli, N. V. Zamfir, and E. A. McCutchan, Phys. Rev. C **73**, 037301 (2006).
[7] B. A. Brown, N. J. Stone, J. R. Stone, I. S. Towner, and M. Hjorth-Jensen, Phys. Rev. C **71**, 044317 (2005).
[8] K. Sugawara-Tanabe and K. Tanabe, Phys. Lett. B **207**, 243 (1988).
[9] A. Ansari, Phys. Rev. C **41**, 782 (1990).
[10] M. L. Cescato, Y. Sun, and P. Ring, Nucl. Phys. **A 533**, 455 (1991).
[11] M. Saha and S. Sen, Nucl. Phys. **A 552**, 37 (1993).
[12] Y. Sun and J. L. Egido, Nucl. Phys. **A 580**, 1 (1994).
[13] V. Velazquez, J. Hirsch, Y. Sun, and M. Guidry, Nucl. Phys. **A 653**, 355 (1999).
[14] Y. Sun, J.-y. Zhang, and M. Guidry, Phys. Rev. C **63**, 047306 (2001).
[15] Y. Sun, J. A. Sheikh, and G.L. Long, Phys. Lett. **B 533**, 253 (2002).
[16] K. Hara and Y. Sun, Int. J. Mod. Phys. **E 4**, 637 (1995).
[17] S. G. Nilsson, C. F. Tsang, A. Sobiczewski, Z. Szymanski, S. Wycech, C. Gustafson, I.-L. Lamm, P. Möller, and B. Nilsson, Nucl. Phys. A **131** (1969) 1.
[18] P. Ring and P. Schuck, *The Nuclear Many Body Problem* (Springer-Verlag, New York, 1980).
[19] F. Iachello and A. Arima, *The Interacting Boson Model* (Cambridge University Press, Cambridge, 1987).
[20] S. Raman, C. W. Nestor, Jr., and P. Tikkanen, At. Data Nucl. Data Tables, **78**, 1 (2001).
[21] B. Castel and I. S. Towner, *Modern Theories of Nuclear Moments* (Clarendon, Oxford, 1990).
[22] Y. Sun and C.-L. Wu, Phys. Rev. C **68**, 024315 (2003).